

# Revisiting for maximal flavor violating $Z'_{e\mu}$ and its phenomenology constraints

Jia Liu,<sup>1,2,\*</sup> Muyuan Song,<sup>2,1,†</sup> and Haohao Zhang<sup>2,‡</sup>

<sup>1</sup>*School of Physics and State Key Laboratory of Nuclear Physics and Technology,  
Peking University, Beijing 100871, China*

<sup>2</sup>*Center for High Energy Physics, Peking University, Beijing 100871, China*

(Dated: July 9, 2024)

## Abstract

Lepton flavor violation (LFV), observed conclusively in neutrino oscillations, remains a pivotal area of investigation due to its absence in the Standard Model (SM). Beyond the Standard Model (BSM) physics explores charged lepton flavor violation (CLFV), particularly through new particle candidates such as the  $Z'$ . This article focuses on maximal LFV interactions facilitated by the  $Z'$  boson, specifically targeting its off-diagonal interactions with the first and second generations of charged and neutral leptons. In our ultraviolet (UV) model for the origin of the  $Z'$ , inspired by the work of [R.Foot *et al.*, Phys.Rev. D50 (1994) 4571-4580], we utilize the discrete  $Z_2$  symmetry to investigate the maximal LFV mediated by the  $Z'$  between the muon ( $\mu$ ) and electron ( $e$ ) arising from the additional scalars. This symmetry prohibits flavor-conserving interactions between  $Z'$  and  $\mu^+\mu^-$ ,  $e^+e^-$ . In conjunction with collider,  $(g-2)_\mu$ ,  $(g-2)_e$ , inverse  $\mu$  decay and LFV decay constraints, we provide forecasts for anticipated limits derived from processes such as  $\nu_\mu N \rightarrow \nu_e \mu^+ e^- N$  in neutrino trident experiments like the DUNE experiment. These limits highlight the prospective scope and significance of LFV investigations within these experimental frameworks. From the range of mass between 0.01 GeV and 10 GeV, the most stringent limit arise from  $\mathcal{B}(\mu \rightarrow e + X + \gamma)$  for  $M_{Z'} < m_\mu$  while neutrino trident processes constrain effectively as  $M_{Z'} \rightarrow 10$  GeV.

---

\*Electronic address: [jialiupku.edu.cn](mailto:jialiupku.edu.cn)

†Electronic address: [muyuansong@pku.edu.cn](mailto:muyuansong@pku.edu.cn)

‡Electronic address: [2101110115@stu.pku.edu.cn](mailto:2101110115@stu.pku.edu.cn)

## Contents

|  |    |
|--|----|
| <b>I. Introduction</b>   | 3  |
| <b>II. Maximal LFV <math>Z'</math> model</b>                               | 4  |
| A. An ultraviolet (UV) model with maximal LFV $Z'$                         | 6  |
| <b>III. LFV limits</b>   | 9  |
| A. $(g - 2)_\mu$ and $(g - 2)_e$   | 10 |
| B. Collider constraints  | 11 |
| C. Muon decay limits   | 13 |
| D. Inverse $\mu$ decay   | 14 |
| E. Muonium-anti Muonium oscillation ( $\text{Mu} - \overline{\text{Mu}}$ ) | 15 |
| F. Neutrino trident production with maximal LFV $Z'$                       | 16 |
| <b>IV. Results</b>   | 19 |
| <b>V. Conclusions</b>  | 21 |
| A. Scalar potential with neutral scalars                                   | 22 |
| B. Kinematic variables for the neutrino trident process.                   | 23 |
| <b>Acknowledgments</b>   | 24 |
| <b>References</b>  | 25 |

## I. INTRODUCTION

Lepton Flavor Violation (LFV) holds considerable significance in particle physics, offering insights into fundamental interactions beyond the Standard Model (SM). The theoretical motivation for searching for LFV processes stems from the possibility that new symmetries might suppress non-conservative leptonic flavor interactions, rendering these phenomena less apparent [1–4]. Investigating LFV in novel particle interactions continues to be a dynamic and compelling area of research, despite the yet unrealized expectations, such as searches for axion-like particles (ALPs) [5–10]. Moreover, LFV studies involving right-handed neutrinos with non-zero mass in SUSY [11, 12], little Higgs models [13, 14], seesaw (with EFT) [15], SMEFT [16, 17], B-LSSM [18] and dark matter [19, 20] have spurred investigations into various lepton flavor violating interactions. In contrast, exploring smaller masses around the electroweak scale has prompted investigations both with and without new gauge symmetries, as highlighted in recent studies such as [21–29], even offering potential explanations for discrepancies observed in quantities like  $(g - 2)_\mu$  [30–32]. There has been significant emphasis on new gauge interactions involving  $U(1)'$ , with researchers actively searching for flavor-conserving interactions between the  $Z'$  boson and leptons, from theoretical studies to experimental investigations [33–35]. Special attention has been given to maximal flavor violation, where off-diagonal couplings are considered dominant, as highlighted in references [23, 36–39]<sup>1</sup>. For experiment searches, neutrino experiments have undertaken several LFV searches, as labeled by references such as [41–43]. In neutrino experiments, the new gauge interaction undergoes testing through a process known as neutrino trident production [44, 45], where an initial neutrino collides with stable nuclei, resulting in the production of a pair of charged leptons. Previous searches have primarily focused on pairs of  $\mu$  with opposing charges [41–43], extending to potential combinations with LHC energy regimes [46, 47] and exploring new physics effects from atmospheric neutrinos [48]. Nevertheless, maximal mixing between  $\mu$  and  $e$  flavors could produce a clear signal without background interference. Such distinct flavor signatures considerably simplify the analysis compared to previous searches. Moreover, proposed explorations on DUNE intend to investigate final states featuring muon-electron pairs within SM [49], thereby augmenting sensitivity to lepton flavor-violating interactions.

---

<sup>1</sup> Indeed, maximal flavor violation has been explored extensively in the quark sector, even in the absence of maximal flavor violation in the lepton sector [40].

From a theoretical standpoint, Ref. [23], emphasized maximal LFV involving the  $Z'\bar{\mu}\tau$  interaction, suggesting equivalence in the effects on the Yukawa couplings  $H\bar{\mu}\mu$  and  $H\bar{\tau}\tau$ . However, recent Higgs measurements contradict this assumption. On the other hand, the recent Higgs decay measurement still survives the scenario where  $H\bar{\mu}\mu, H\bar{e}e$  couplings to be identical in the presence of LFV  $Z'\mu^\pm e^\mp$  within similar models. Therefore, exploring  $\mu$  and  $e$  flavor interactions proves crucial for advancing LFV investigations from both experimental and theoretical perspectives.

In this study, we explore the implications of neutrino trident production limits on maximal LFV involving  $Z'$  in the DUNE experiment. We demonstrate that the neutrino trident process sets stringent constraints on LFV interactions between  $\mu$  and  $e$  compared to collider experiments (LEP and Belle-II) and other LFV interaction limits, particularly in the mass range  $m_\mu < M_{Z'} < 10$  GeV. In the lower mass regime, the most restrictive limit originates from the inclusive search for the  $\mathcal{B}(\mu \rightarrow e + \gamma + X)$  process when  $M_{Z'} < m_\mu$ .

The paper is structured as follows: Section II clarifies the simplified  $Z'$  model, emphasizing its dominant new off-diagonal gauge interaction and discussing its implications for charged and neutral leptons. Additionally, we introduce a UV model in Section II that comprises three scalar doublets and an additional singlet, where the singlet is pivotal in providing mass for the maximal LFV  $Z'$ . Section III addresses the LFV constraints on  $Z'$ , incorporating findings from collider experiments, LFV  $\mu$  decays, neutrino-charged lepton scattering (inverse  $\mu$  decay), and the neutrino trident process. Additionally, we analyze the implications of LFV couplings for  $(g-2)_{\mu,e}$ . In Section IV, we depict exclusion limit plots derived from the couplings between  $Z'$  and leptons. Finally, Section V concludes with a discussion on future prospects.

## II. MAXIMAL LFV $Z'$ MODEL

In models incorporating an additional  $Z'$  boson, maintaining a global anomaly-free symmetry is essential within the SM framework. Previous studies of such models have concentrated on interactions between the  $Z'$  boson and leptons, highlighting scenarios where a discrete symmetry prevents diagonal couplings [23]. This precaution is crucial to prevent mixing between the  $A$  and  $Z'$  bosons, as described by transformations within the kinetic

Lagrangian,

$$\mathcal{L} = -\frac{1}{4}F_{\mu\nu}F^{\mu\nu} - \kappa F_{\mu\nu}F'^{\mu\nu} - \frac{1}{4}F'_{\mu\nu}F'^{\mu\nu}, \quad (1)$$

where  $B_\mu \rightarrow B_\mu$ ,  $Z'_\mu \rightarrow -Z'_\mu$ . Under the  $Z_2$  discrete symmetry, the above mixing between  $A$  and  $Z'$  is forbidden.

To satisfy the anomaly-free requirements, we assign distinct  $U(1)'$  charges to different generations of leptons. Specifically, we consider a scenario where these  $U(1)'$  charge assignments apply to the first and second generations while the third generation remains uncharged under  $U(1)'$ . Alternatively, opposite charges could be assigned to any other pair of generations, such as  $\mu/\tau$  or  $e/\tau$ . In such cases, the flavor states under  $SU(3) \times SU(2) \times U(1)_Y \times U(1)'$  are structured as described in Ref. [23],

$$\begin{aligned} \ell_{1L} &= \frac{(e + \mu)_L}{\sqrt{2}}, \ell_{2L} = \frac{(e - \mu)_L}{\sqrt{2}}, e_{1R} = \frac{(e + \mu)_R}{\sqrt{2}}, e_{2R} = \frac{(e - \mu)_R}{\sqrt{2}}, \\ \ell_{1L} &\sim (\mathbf{1}, \mathbf{2})(-1, 2a), \ell_{2L} \sim (\mathbf{1}, \mathbf{2})(-1, -2a), \\ e_{1R} &\sim (\mathbf{1}, \mathbf{1})(-2, 2a), e_{2R} \sim (\mathbf{1}, \mathbf{1})(-2, -2a), \end{aligned} \quad (2)$$

where  $a$  is a parameter for the  $U(1)'$  charge,  $\ell_{1L,2L}$  and  $e_{1R,2R}$  are the flavor states, while  $e$  and  $\mu$  are the eigenstates in the mass basis. With the discrete symmetry ( $\ell_{1L} \rightarrow \ell_{2L}$ ,  $e_{1R} \rightarrow e_{2R}$ ,  $Z'_\mu \rightarrow -Z'_\mu$ ) in place, the interaction between  $Z'$  and flavor states would demonstrate the maximal mixing feature for lepton mass states:

$$\mathcal{L}_{\text{NC}}^{Z'} = g_{e\mu} Z'_\mu (\bar{\mu} \gamma^\mu e + \bar{e} \gamma^\mu \mu), \quad (3)$$

and neutrino- $Z'$  interaction,

$$\mathcal{L}_{\text{NC}}^{Z'} = g_{e\mu} Z'_\mu (\bar{\nu}_{\mu L} \gamma^\mu \nu_{e L} + \bar{\nu}_{e L} \gamma^\mu \nu_{\mu L}), \quad (4)$$

where the  $Z'$  does not couple to the diagonal term in the mass basis.

Next, the decay width of the  $Z'$  can be straightforwardly calculated from the above interaction, considering the limit where  $m_e \rightarrow 0$ ,

$$\Gamma(Z' \rightarrow e^\pm \mu^\mp) = \frac{g_{e\mu}^2 (M_{Z'}^2 - m_\mu^2)^2 (2M_{Z'}^2 + m_\mu^2)}{24\pi M_{Z'}^5}, \quad (5)$$

$$\Gamma(Z' \rightarrow \nu_{e(\mu)} \bar{\nu}_{\mu(e)}) = \frac{g_{e\mu}^2 M_{Z'}}{24\pi}, \quad (6)$$

Fig. 1 depicts the decay widths of  $Z'$  across a mass range from 0.01 GeV to 10 GeV, with  $g_{e\mu} = 10^{-2}$  (solid line) and  $10^{-4}$  (dashed line). It becomes apparent that the two decay

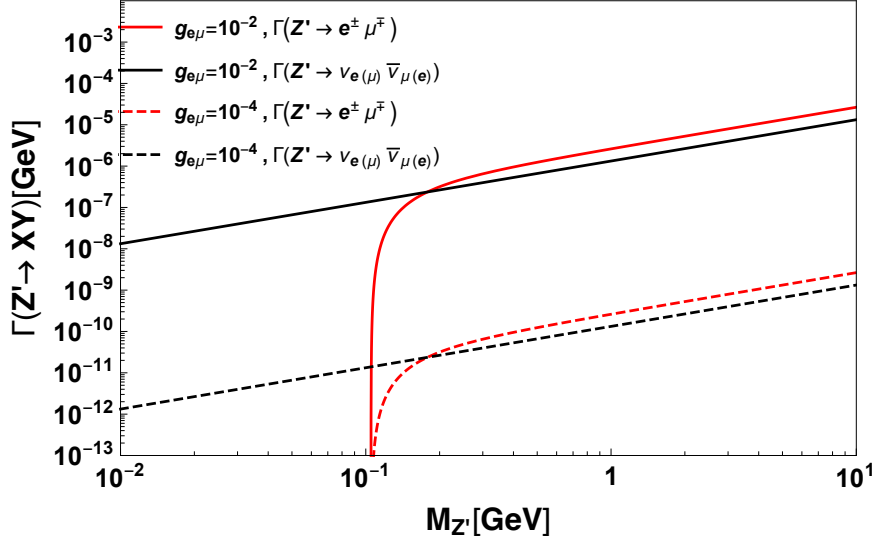


FIG. 1: The decay width of  $Z'$  correlated with charged and neutral leptons with  $g_{e\mu} = 10^{-2}$ (solid),  $10^{-4}$ (dashed). The red lines label the  $\Gamma(Z' \rightarrow e^\pm \mu^\mp)$  and the black lines label the  $\Gamma(Z' \rightarrow \nu_{e(\mu)} \bar{\nu}_{\mu(e)})$ .

channels become comparable when  $M_{Z'}$  is significantly larger than  $m_\mu + m_e$ . Furthermore, for large  $M_{Z'}$ , the decay width into neutrinos is half that of the charged lepton decay,

$$2 \mathcal{B}(Z' \rightarrow \nu_{e(\mu)} \bar{\nu}_{\mu(e)}) = \mathcal{B}(Z' \rightarrow e^\pm \mu^\mp). \quad (7)$$

because the neutrinos only have left-handed spinors.

### A. An ultraviolet (UV) model with maximal LFV $Z'$

The preceding section examines a simplified LFV  $Z'$  and explores its new gauge interaction. This prompts the inquiry into how such a  $Z'$  could be generated within a UV framework. In our UV model, we establish the existence of a model comprising three scalar doublets and an additional real singlet, with specific charge assignments outlined in Tab. I as extended by Ref. [23].

The electromagnetic neutral components of three scalar doublets and one singlet are given in the following,

$$\begin{aligned} \phi_1 &\supset v_1 + (\rho_1 + i\eta_1) / \sqrt{2}, \phi_2 \supset v_2 + (\rho_2 + i\eta_2) / \sqrt{2}, \\ \phi_3 &\supset v_3 + (\rho_3 + i\eta_3) / \sqrt{2}, \phi_4 = v_4 + \rho_4 / \sqrt{2}, \end{aligned} \quad (8)$$

| Group     | $\ell_{1L}$ | $\ell_{2L}$ | $e_{1R}$ | $e_{2R}$ | $\phi_1$ | $\phi_2$ | $\phi_3$ | $\phi_4$ |
|-----------|-------------|-------------|----------|----------|----------|----------|----------|----------|
| $SU(3)_c$ | <b>1</b>    | <b>1</b>    | <b>1</b> | <b>1</b> | <b>1</b> | <b>1</b> | <b>1</b> | <b>1</b> |
| $SU(2)_L$ | <b>2</b>    | <b>2</b>    | <b>1</b> | <b>1</b> | <b>2</b> | <b>2</b> | <b>2</b> | <b>1</b> |
| $U(1)_Y$  | -1          | -1          | -2       | -2       | 1        | 1        | 1        | 0        |
| $U(1)'$   | 2a          | -2a         | 2a       | -2a      | -4a      | 4a       | 0        | 1        |

TABLE I: Particle contents and charges in the  $U(1)'$  model with  $\ell_{1L,2L}, e_{1R,2R}$  and four scalars  $\phi_{1,2,3,4}$ .

where we will propose the discrete symmetry  $1 \leftrightarrow 2$  ( $\ell_{1L} \rightarrow \ell_{2L}, e_{1R} \rightarrow e_{2R}, \phi_1 \rightarrow \phi_2$ ), thereby enforcing  $v_0 \equiv v_1 = v_2$ . In contrast to Ref. [23], we introduced an additional singlet scalar  $\phi_4$ , which is charged solely under  $U(1)'$ . The possible scalar potential is given in Appendix A.

On the other side, the different generation of leptons have exactly opposite charges under  $U(1)'$  in Table I, which ensures the anomaly free condition. Therefore, the Yukawa interaction for leptons under the above charge assignments would be expressed as follows [23],

$$\begin{aligned} \mathcal{L}_{\text{Yukawa}}^{\ell} = & \mathcal{Y}_1 \bar{\ell}_{1L} e_{1R} \phi_3 + \mathcal{Y}_1 \bar{\ell}_{2L} e_{2R} \phi_3 + \mathcal{Y}_3 \bar{\ell}_{3L} e_{3R} \phi_3 \\ & + \mathcal{Y}_{12} (\bar{\ell}_{1L} e_{2R} \phi_2 + \bar{\ell}_{2L} e_{1R} \phi_1) + \text{h.c.} \end{aligned} \quad (9)$$

where the Yukawa sector obeys the discrete symmetry  $1 \leftrightarrow 2$ . The scalar  $\phi_4$  does not participate in Yukawa interactions due to its specific charge assignment. Instead, it contributes solely to the mass generation of the  $Z'$  boson through the process of symmetry breaking. As detailed in Appendix A, the mass eigenstate  $H$  emerges from the diagonalization of mass matrices, particularly when the flavor state  $\rho_3$  aligns with the physical state  $H$ , facilitated by setting  $\lambda_4 \rightarrow 0$ . The SM-like Higgs ( $H$ ) exhibits Yukawa couplings with leptons as follows,

$$\mathcal{L}_H^{\ell} = \frac{m_{\tau}}{\sqrt{2}v_3} \bar{\tau} \tau H + \frac{m_{\mu} + m_e}{2\sqrt{2}v_3} (\bar{\mu} \mu + \bar{e} e) H, \quad (10)$$

where the off-diagonal Yukawa terms vanish. This cancellation occurs because the terms

$(\bar{\ell}_{1L}e_{2R})$  and  $(\bar{\ell}_{2L}e_{1R})$  eliminate the off-diagonal contributions:

$$\begin{aligned}
& \bar{\ell}_{1L}e_{2R}\phi_2 + \bar{\ell}_{2L}e_{1R}\phi_1 + \text{h.c} \\
&= \frac{1}{2\sqrt{2}}(\bar{e}_L e_R \mathcal{Y}_{12} + \bar{e}_L \mu_R \mathcal{Y}_{12} - \bar{\mu}_L e_R \mathcal{Y}_{12} - \bar{\mu}_L \mu_R \mathcal{Y}_{12})\rho_1 \\
&+ \frac{1}{2\sqrt{2}}(\bar{e}_L e_R \mathcal{Y}_{12} - \bar{e}_L \mu_R \mathcal{Y}_{12} + \bar{\mu}_L e_R \mathcal{Y}_{12} - \bar{\mu}_L \mu_R \mathcal{Y}_{12})\rho_2 \\
&+ \frac{\sqrt{2}}{2}(\bar{e}_L e_R \mathcal{Y}_1 + \bar{\mu}_L \mu_R \mathcal{Y}_1)\rho_3 + \text{h.c.}
\end{aligned} \tag{11}$$

Applying the linear transformation from  $\rho_1, \rho_2$  to the neutral states  $S_1, S_2$ ,

$$S_1 = \frac{\rho_1 + \rho_2}{\sqrt{2}}, S_2 = \frac{\rho_1 - \rho_2}{\sqrt{2}}, \tag{12}$$

results in the elimination of off-diagonal Yukawa-type interactions involving  $S_1$ . All off-diagonal interactions are transferred to the additional scalar  $S_2$ , which we note could be significantly heavier due to large number of parameters from scalar potential and thus not of primary interest in this context. The Yukawa couplings from the Lagrangian above display a distinctive feature wherein the couplings for  $\mu$  and  $e$  are identical. In Ref. [23], the model presents a unique aspect where the Yukawa couplings between  $H - \bar{\mu}\mu$  and  $H - \bar{\tau}\tau$  are equal. However, the measurement of Higgs decay to muon and tau leptons have already ruled out this possibility [50, 51]. Hence, our attention is directed exclusively towards the mixing between  $\mu$  and  $e$ , given the current relatively low precision in measurements of  $H - \bar{\mu}\mu$  and  $H - \bar{e}e$ . Latest measurements of the branching ratios for  $\mathcal{B}(H \rightarrow \mu^+\mu^-) < 2.6 \times 10^{-4}$  by ATLAS [50] and  $\mathcal{B}(H \rightarrow e^+e^-) < 3 \times 10^{-4}$  by CMS [52] suggest that setting the Yukawa couplings for both electrons and muons to  $\mathcal{Y}_e \sim \mathcal{Y}_\mu < \mathcal{O}(10^{-4})$  would not impose stringent constraints on the model.

Conversely, following the transformation in eq. (12), the CP-even squared mass matrices result in  $S_1, \rho_3$  being non-diagonal when  $\lambda_4 \neq 0$ , indicating that  $S_1, \rho_3$  are not mass eigenstates. Instead, after diagonalization (as shown in eqs. (A7 and A8)), the mass eigenstates are  $S'_1, H$  respectively. The transformation from flavor states  $(\rho_1, \rho_2, \rho_3, \rho_4)$  to mass states  $(S'_1, S_2, H, S_4)$  leads to the new SM Yukawa interaction between  $H$  and leptons, represented as follows (where  $S_2$  and  $S_4$  are already the mass eigenstates):

$$\mathcal{L}_H^\ell = \frac{m_\tau}{\sqrt{2}v_3}\bar{\tau}\tau H + \left[ \frac{m_e + m_\mu}{2\sqrt{2}v_3} + \frac{\lambda_4^2}{(\lambda_1 + \lambda_4)^2} \frac{v_0}{v_3} \frac{m_\mu - m_e}{2\sqrt{2}v_3} \right] \bar{\mu}\mu H \tag{13}$$

$$+ \left[ \frac{m_e + m_\mu}{2\sqrt{2}v_3} + \frac{\lambda_4^2}{(\lambda_1 + \lambda_4)^2} \frac{v_0}{v_3} \frac{m_e - m_\mu}{2\sqrt{2}v_3} \right] \bar{e}e H, \tag{14}$$

Once again, the off-diagonal interaction terms vanish for the same reasons as previously mentioned. It is noteworthy that the Yukawa couplings between  $H$  and  $\mu, e$  are no longer identical. However, directly converting the formal expression back to the SM  $\mu$  and  $e$  Yukawa couplings would require setting  $v_0 = v_3$ , which would affect the Yukawa couplings for other fermions, such as the  $\tau$  Yukawa coupling. Instead, simplifying this scenario involves setting  $\lambda_4 = 0$  to reduce one parameter of the model. In this case, the Yukawa couplings for  $\mu$  and  $e$  become nearly equivalent and revert to the formal condition in Eq. (10).

From the  $U(1)'$  covariant derivative ( $D_\mu = \partial_\mu + ig'Q_{U(1)'}Z'_\mu$ ), the gauge interaction between  $Z'$  and lepton flavor states can be easily expressed as follows,

$$\mathcal{L}_{\text{gauge}}^{Z'} = g_{e\mu}(\bar{\ell}_{1L}\gamma^\mu\ell_{1L} - \bar{\ell}_{2L}\gamma^\mu\ell_{2L} + \bar{e}_{1R}\gamma^\mu e_{1R} - \bar{e}_{2R}\gamma^\mu e_{2R}), \quad (15)$$

where  $g_{e\mu} = g' 2a$  is the product of charge and coupling under the  $U(1)'$ . According to the  $U(1)'$  charge assignments,  $\phi_3$  would not couple with  $U(1)'$  gauge boson and  $\phi_4$  only connects with  $Z'$ . After electroweak symmetry breaking associated with  $U(1)'$ , the masses of the SM  $Z$  boson and  $Z'$  are determined from the covariant derivative,

$$\begin{aligned} |D_\mu\phi_1|^2 + |D_\mu\phi_2|^2 + |D_\mu\phi_3|^2 &\supset \frac{1}{2}M_Z^2Z^\mu Z_\mu, \\ |D_\mu\phi_1|^2 + |D_\mu\phi_2|^2 + |D_\mu\phi_4|^2 &\supset \frac{1}{2}M_{Z'}^2Z'^\mu Z'_\mu, \\ M_Z^2 = \frac{1}{4}(g^2 + g_Y^2)(v_3^2 + 2v_0^2), \quad M_{Z'}^2 &\sim g_{e\mu}^2(2v_0^2 + v_4^2) \sim g_{e\mu}^2 v_{Z'}^2. \end{aligned} \quad (16)$$

where  $v_0 < v_3$ . By taking  $(v_3^2 + 2v_0^2) \approx v_{\text{SM}}^2$ , this ensures that  $M_Z$  remains unchanged while allowing  $M_{Z'}$  to be a free parameter through varying the value of  $v_{Z'}$ . In comparison to Ref. [23], their model features  $M_{Z'}$  strongly constrained by  $M_Z$ , resulting in no available region due to both Higgs-Yukawa and  $M_Z$  constraints.

### III. LFV LIMITS

In this section, our attention turns to the phenomenology of low mass  $Z'$ , where we conduct a thorough analysis to constrain  $g_{e\mu}$  and  $M_{Z'}$ . Initially, we consider the anomalous magnetic moment ( $g - 2$ ) of the muon/electron and the constraints provided by electron-positron colliders such as the Belle-II experiment and LEP measurements. Then, we consider the LFV decays ( $\mu$  decays) since the majority interaction between  $Z'$  with leptons are  $\mu$  and  $e$ . Thirdly, inverse  $\mu$  decay and Muonium-anti Muonium oscillation are taking into account.

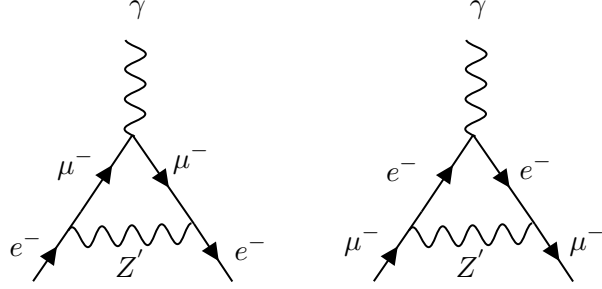


FIG. 2: The representative Feynman diagrams for  $(g-2)_{e/\mu}$  contribution via the LFV  $Z'$  interaction.

Finally, the neutrino trident process would be discussed and we will present the difference between SM process and distinctive signal from the new  $Z'$  contribution.

### A. $(g-2)_\mu$ and $(g-2)_e$

According to the window observable theory [53, 54] and the SM prediction [55], the current disagreement concerning the  $\Delta a_\mu$  designations has emerged as follows [55–58]:

$$\Delta a_\mu^{\text{window}} = (1.81 \pm 0.47) \times 10^{-9}, \quad (17)$$

On the other hand, the electron magnetic dipole moment [59] with its experiment measurement through Rb in 2020 [60, 61], the discrepancy with SM prediction can be expressed as follows:

$$\Delta a_e^{\text{Rb}} = 34(16) \times 10^{-14}, \quad (18)$$

whereas the Cs atoms measurement method search has obtained a lower bound [62],

$$\Delta a_e^{\text{Cs}} = -102(26) \times 10^{-14}, \quad (19)$$

The LFV coupling  $(g_{ij})$  would thus contribute to  $(g-2)$  with the Fig. 2 and its contribution calculated through package-X [63] via the following expression,

$$\Delta a_e = \frac{g_{e\mu}^2 m_e m_\mu \left( -m_\mu^6 + 4M_{Z'}^6 - 3m_\mu^3 M_{Z'}^4 - 6m_\mu^3 M_{Z'}^4 \log\left(\frac{M_{Z'}^2}{m_\mu^2}\right) \right)}{16\pi^2 M_{Z'}^2 (M_{Z'}^2 - m_\mu^2)^3}, \quad (20)$$

$$\Delta a_\mu = \frac{g_{e\mu}^2}{16\pi^2} \left( -\frac{(2M_{Z'}^2 - m_\mu^2)^2}{m_\mu^2 M_{Z'}^2} - \frac{2M_{Z'}^2 (3m_\mu^2 - 2M_{Z'}^2) \log\left(\frac{M_{Z'}^2}{|M_{Z'}^2 - m_\mu^2|}\right)}{m_\mu^4} \right). \quad (21)$$

We apply the  $2\sigma$  bounds based on the recent measurements of eqs. (17 and 18) to separately illustrate  $\Delta a_\mu$  and  $\Delta a_e$ .

## B. Collider constraints

For an electron-positron collider, particularly the Belle-II experiment, the search for LFV  $Z'$  bosons is linked with  $e\mu + \cancel{E}$  final states. We use their constraints on the product of the cross-section  $\sigma(e^+e^- \rightarrow \mu^\pm e^\pm + \cancel{E})$  (see Fig. 3) and the detector efficiency  $\epsilon$  to set the upper bound [64]. We used the product  $(\epsilon \times \sigma)$  to constrain the coupling in the mass region up to approximately 8 GeV. The numerical cross-section for the  $Z'$  is directly proportional to  $g_{e\mu}^2$  and can be computed by solving the relation between the existing product limit and their selection of  $M_{Z'}$  values.

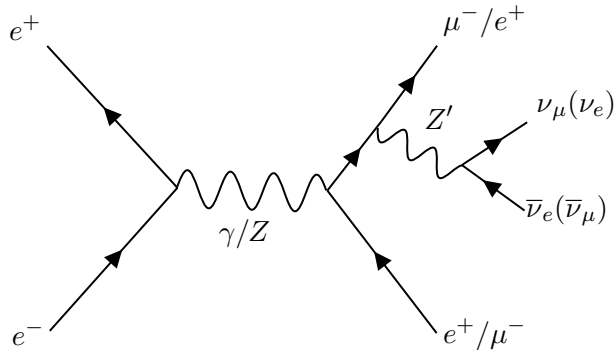


FIG. 3: Typical Feynman diagrams for  $e^+e^- \rightarrow e^\pm\mu^\mp + \cancel{E}$ .

In the process  $e^+e^- \rightarrow \mu^+\mu^-$  [65], the LFV interaction occurs via a  $t$ -channel exchange mediated by  $M_{Z'}$ . As reported in the aforementioned reference, LEP conducted measurements of this process at  $\sqrt{s} = 189$  GeV. The background from the  $s$ -channel in the SM (mediated by  $H$  bosons) is suppressed by  $m_\mu m_e / M_H^2$  due to small Yukawa couplings, resulting in significant interference contributions between new physics and the SM background

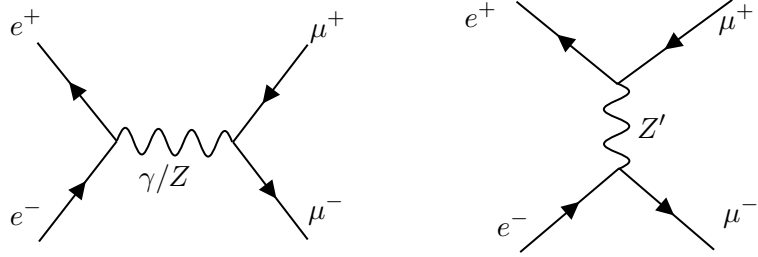


FIG. 4: Typical Feynman diagrams for  $e^+e^- \rightarrow \mu^+\mu^-$ . Left panel: SM contribution. Right panel:  $Z'$  contribution.

associated only with s-channel ( $\gamma$  and  $Z$ ) diagrams ( $\mathcal{M}_{\text{total}} = \mathcal{M}_{Z'(t)} + \mathcal{M}_{\gamma(s)} + \mathcal{M}_{Z(s)}$ ) as depicted in Fig. 4.

The cross-section of the process expands the terms to  $\mathcal{O}(s^{-1})$  as follows:

$$\sigma(e^+e^- \rightarrow \mu^+\mu^-) = \frac{e^4(1+24s_w^4)}{768\pi s_w^4(1-s_w^2)^2 s} + \frac{e^2 g_{e\mu}^2 (1+4s_w^2)(2\log(s/M_{Z'}^2) - 3)}{64\pi s_w^2(1-s_w^2) s} + \frac{g_{e\mu}^4}{4\pi M_{Z'}^2}. \quad (22)$$

The squared amplitude of the new physics process is proportional to  $1/(t - M_{Z'}^2)^2$ , where the variable  $t$  depends on the scattering angle  $\theta$ . Upon integrating over  $\theta$ , the cross-section becomes proportional to the  $1/(t - M_{Z'}^2)$  term. Consequently, this factor reaches its maximum value of  $1/M_{Z'}^2$  when  $t$  approaches zero. Furthermore, the contribution from the term  $q^\mu q^\nu/M_{Z'}^2$  is proportional to  $m_\mu^4/(M_{Z'}^4 s)$ , which is negligible compared to the  $1/M_{Z'}^2$  contribution associated with the term  $g^{\mu\nu}$  in the region of interest for  $M_{Z'}$ . In summary, the factor  $1/M_{Z'}^2$  in the aforementioned equation arises from the t-channel in the context of new physics.

We conducted an analysis of the LEP cross-sections [65] at  $\sqrt{s} = 189$  GeV, corresponding to an integrated luminosity of  $155.21 \text{ pb}^{-1}$ . This analysis encompasses the range of  $\cos \theta$  from  $-0.97$  to  $0.97$ , partitioned into 10 bins, in order to establish constraints on the  $Z'$  boson. This enables us to perform a  $\chi^2$  test based on the differential cross-section of the process (denoted as  $N_{\text{signal}}^j = \int d\sigma/d\cos \theta \times \mathcal{L}$ ),

$$\chi^2 = \sum_{j=1}^{10} \frac{(N_{\text{experiment}}^j - (N_{\text{background}}^j + N_{\text{signal}}^j))^2}{(\sigma_{\text{error}}^j)^2}. \quad (23)$$

where  $N_{\text{experiment}}^i$  represents the number of events measured by the LEP, and  $N_{\text{background}}^i$  represents the difference between the theoretical predictions and the measured events in each bin. The two independent parameters,  $g_{e\mu}$  and  $M_{Z'}$ , can then be constrained using the 10 bins with  $\chi^2 \leq 5.991$  (95% CL).

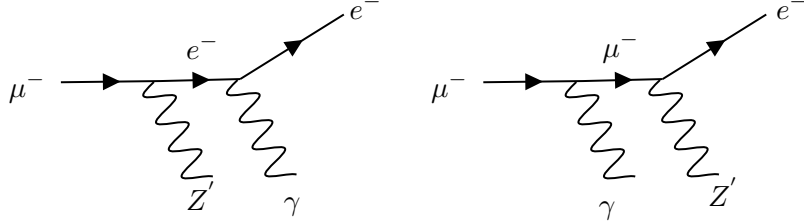


FIG. 5: The representative Feynman diagrams for 3-body decay of the muon which  $Z'$  is lighter than  $m_\mu$ .

### C. Muon decay limits

The occurrence of LFV decays, characterized as  $\ell_i \rightarrow \ell_j + X$ , imposes constraints on the underlying interactions. In the context of muon decays, such as  $\mu \rightarrow e\gamma$ ,  $\mu \rightarrow 3e$  and  $\mu \rightarrow e + X$  (A summarized overview is provided in [66]), these processes define significant boundaries for new physics. Notably, the  $\mu \rightarrow e\gamma$  decay has been scrutinized extensively at the MEG experiment [67–69], while  $\mu \rightarrow 3e$  has been explored by various experiments [70–72]. Additionally,  $\mu \rightarrow e + X$  processes have been investigated by the TWIST collaboration [73]. The absence of kinetic mixing, such as  $Z - Z'$  or  $A - Z'$  interactions, precludes the occurrence of  $\mu \rightarrow 3e$  due to the lack of diagonal coupling vertices between  $Z'$  and charged leptons. Consequently, the constraints on LFV decays primarily focus on two-body processes, where the final decay channel involves  $\mu \rightarrow eZ'$  and subsequent  $Z'$  decays exclusively to neutrinos with a branching ratio of 100%. The TWIST experiment utilized muon stopped events to establish an upper limit for  $\mathcal{B}(\mu \rightarrow e + X)$  of approximately  $\mathcal{O}(10^{-5})$  within the mass region of  $X$ , ranging from 13 MeV to 80 MeV [73]. In addition, the PSI experiment with a HPGe detector, testing masses ranging from 100 MeV to 150 MeV, obtained an upper limit of  $\mathcal{B}(\mu^+ \rightarrow e^+ + X) < 5.7 \times 10^{-4}$  [74]. Therefore, we will employ the current limit established by the TWIST collaboration to assess the constraint on the  $Z'$ .

The decay width of  $\mu \rightarrow e + Z'$  can be expressed as follows under the approximation of neglecting  $m_e$ ,

$$\Gamma(\mu \rightarrow e + Z') = \frac{g_{e\mu}^2 (m_\mu^6 - 3m_\mu^2 M_{Z'}^4 + 2M_{Z'}^6)}{16\pi m_\mu^3 M_{Z'}^2}, \quad (24)$$

with its branching ratio ( $\tau_\mu = 2.2 \times 10^{-6} s \sim \Gamma_\mu = 3 \times 10^{-19} \text{ GeV}$ ) [75],

$$\mathcal{B}(\mu \rightarrow e + Z') = \Gamma(\mu \rightarrow e + Z')/\Gamma_\mu, \quad (25)$$

However, as reported by Ref. [66], the Crystal Box collaboration [76] has showcased the capability to examine the inclusive  $\mu \rightarrow e + \gamma + X$  decay process with  $\mu \rightarrow e + \gamma$ . They have established an upper bound for the branching ratio  $\mathcal{B}(\mu \rightarrow e + \gamma + X) < 1.3 \times 10^{-9}$  [76]. The three-body decay,  $\mu \rightarrow e + \gamma + X$ , can be expressed as follows,

$$\Gamma(\mu \rightarrow e + \gamma + Z') \simeq \frac{\alpha_{\text{EM}} g_{e\mu}^2 m_\mu^5}{128\pi^2 E_\gamma^2 M_{Z'}^2}. \quad (26)$$

where  $E_\gamma$  correspond to minimum energy cut to prevent infrared divergence (typical energy is picked for 38 MeV in [76]). For  $M_{Z'}$  reduces to  $m_e$ , the decay process is predominantly governed by  $m_\mu$ , leading to tighter constraints on its coupling. Conversely, as the mass of  $Z'$  approaches  $m_\mu$ , the situation is reversed. This is due to the enhancement of  $m_\mu^3/M_{Z'}^2$  (arising from the longitudinal polarization mode of  $Z'$ ), which has been extensively discussed for many channels based on the Goldstone Boson Equivalence Theorem (e.g.,  $\tau \rightarrow \mu Z'$ ,  $t \rightarrow bW^+$  [77–80]). Meanwhile, an additional  $\alpha_{\text{EM}}$  factor and the three body phase space factor further suppresses the new physics contribution compared to the  $\mu \rightarrow e + Z'$  process. Thus, the three-body channel would then be the most stringent limit compares with the two-body channel.

#### D. Inverse $\mu$ decay

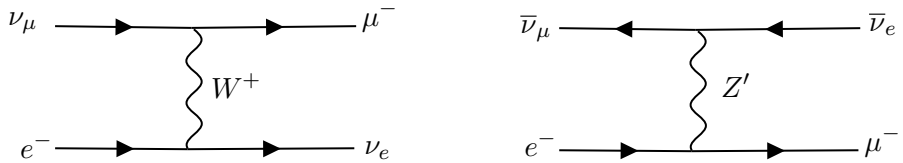


FIG. 6: Feynman diagrams for inverse  $\mu$  decay with the SM electroweak interaction and the LFV  $Z'$  interaction.

In Ref. [81, 82], CHARM and NuTeV collaborations tested the inverse  $\mu$  decay  $\nu_\mu e^- \rightarrow \mu^- \nu_e$  and  $\bar{\nu}_\mu e^- \rightarrow \mu^- \bar{\nu}_e$ , established the upper limit for the ratio of the process as Fig. 6 (where there is no SM contribution for the second channel),

$$R_{\nu e} = \frac{\sigma(\bar{\nu}_\mu e^- \rightarrow \mu^- \bar{\nu}_e)}{\sigma(\nu_\mu e^- \rightarrow \mu^- \nu_e)} < \begin{cases} 0.09 \text{ (90\% C.L.)} & [81] \\ 0.017 \text{ (90\% C.L.)} & [82] \end{cases}, \quad (27)$$

In fact, there is an additional *u*-channel diagram from  $Z'$  contribution supply for the  $\nu_\mu e^- \rightarrow \mu^- \nu_e$  despite the SM ( $W$ ) diagram. However, compared to the SM contribution, the  $Z'$  contribution can be neglected. Therefore, the resulting ratio can be simplified as follows:

$$\frac{\sigma(\bar{\nu}_\mu e^- \rightarrow \mu^- \bar{\nu}_e)}{\sigma(\nu_\mu e^- \rightarrow \mu^- \nu_e)} \simeq \frac{g_{e\mu}^4}{2 G_F^2 M_{Z'}^2 s}, (M_{Z'} < \sqrt{s}), \quad (28)$$

$$\frac{\sigma(\bar{\nu}_\mu e^- \rightarrow \mu^- \bar{\nu}_e)}{\sigma(\nu_\mu e^- \rightarrow \mu^- \nu_e)} \simeq \frac{g_{e\mu}^4}{3 G_F^2 M_{Z'}^4}, (M_{Z'} > \sqrt{s}). \quad (29)$$

where  $\sqrt{s} \approx \sqrt{2E_{\nu_\mu} m_e}$ . In this study, the limit was established by the newest NuTeV search.

### E. Muonium-anti Muonium oscillation ( $\text{Mu} - \overline{\text{Mu}}$ )

One specific observable, Muonium (Mu), forming a bound state of  $\mu^+ e^-$ , would be relevant for exploring new physics, as it could induce Muonium-anti Muonium transitions due to the mediation of the  $Z'$  between two bound states (e.g.,  $\mu^+ + e^- \rightarrow \mu^- + e^+$  in Fig. 7.) [38, 83].

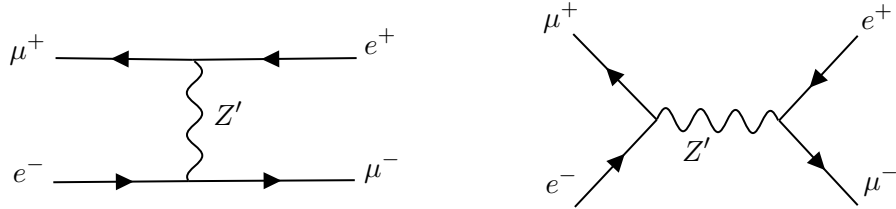


FIG. 7: Feynman diagrams for muonium (Mu) bound state.

This transition probability has been tested by the PSI experiment [84], and its expression could be labeled as follows (only vector current and left/right-handed vertices are the same result in the constraint only proportional to  $g_{e\mu}^2/M_{Z'}^2$ ),

$$P = \frac{2.57 \times 10^{-5}}{G_F^2} (|c_{0,0}|^2 - G_3 + G_{123}|^2 + |c_{1,0}|^2 |G_3 + G_{123}|^2) < 8.3 \times 10^{-11} \quad (30)$$

with parameters,

$$G_1 = G_2 = \sqrt{2} \frac{g_{e\mu}^2}{8M_{Z'}^2}, G_3 = \sqrt{2} \frac{2g_{e\mu}^2}{8M_{Z'}^2}, G_{123} = \frac{G_1 + G_2 - 1/2 G_3}{\sqrt{1 + X^2}}. \quad (31)$$

In the above equations  $|c_{0,0}|^2 = 0.32$  and  $|c_{1,0}|^2 = 0.18$  represent the population states of the Mu [83] and  $X = 6.31 \times B/\text{Tesla}$ , with  $B = 0.1$  Tesla [84]. By using the above transition probability, we can set limits on the  $Z'$  couplings.

## F. Neutrino trident production with maximal LFV $Z'$

Neutrino trident production [44, 45, 85–87], where a neutrino collides with the electric field of a nucleus and produces a pair of charged leptons, is a rare process involving neutral and charged lepton electroweak interactions. This phenomenon has been investigated by several experimental groups, as listed in Table II. It is worth noting that the proposed SHiP experiment [88, 89] will be sensitive to LFV in future searches. Additionally, these processes probe new types of interactions mediated by particles beyond the SM, such as the LFV  $Z'$  boson. Previous experiments have concentrated on utilizing produced  $\mu^+\mu^-$  pairs to constrain the couplings of  $Z'$  with leptons. These searches involving  $Z'$  consider both off-diagonal couplings between different flavors and diagonal couplings with the same flavor. The main challenge lies in distinguishing the new physics signal from significant SM backgrounds, where final states could include  $e^+e^-\nu$ ,  $\mu^+\mu^-\nu$ , or  $e^+\mu^-\nu$ , as shown in the lower figures of Fig. 8. However, the incoming  $\nu_\mu$  beam also provides sensitivity to  $\mu^+e^-\nu$ , a final state not produced by SM. For instance, the DUNE experiment [90] distinguishes between incoming  $\nu_\mu$  and  $\bar{\nu}_\mu$  fluxes, facilitating the isolation of final lepton states. Hence, it offers a clear signal for searches involving the  $Z'\mu^+e^-$  vertex, as shown in the upper two figures of Fig. 8.

| Experiment              | $E_{\nu_\mu}^{\text{mean}}$ (GeV) | Target                |
|-------------------------|-----------------------------------|-----------------------|
| CHARM-II [41, 91]       | $\sim 24$                         | silicon (Z=14,A=28)   |
| CCFR [42, 92–94]        | 160                               | iron (Z=26,A=56)      |
| NuTeV [43, 82]          | 140                               | iron (Z=26,A=56)      |
| DUNE [49, 90, 95]       | $\sim 40$                         | argon (Z=18,A=40)     |
| SHiP(proposed) [88, 89] | $\sim 40$                         | Tungsten (Z=74,A=184) |

TABLE II: Previous and proposed experiments on neutrino tridents along with their respective setup configurations.

The amplitude for the distinctive clean signal channel  $(\nu_\mu(k_1) + \gamma(q) \rightarrow \nu_e(k_2) + \mu^+(p_1) +$

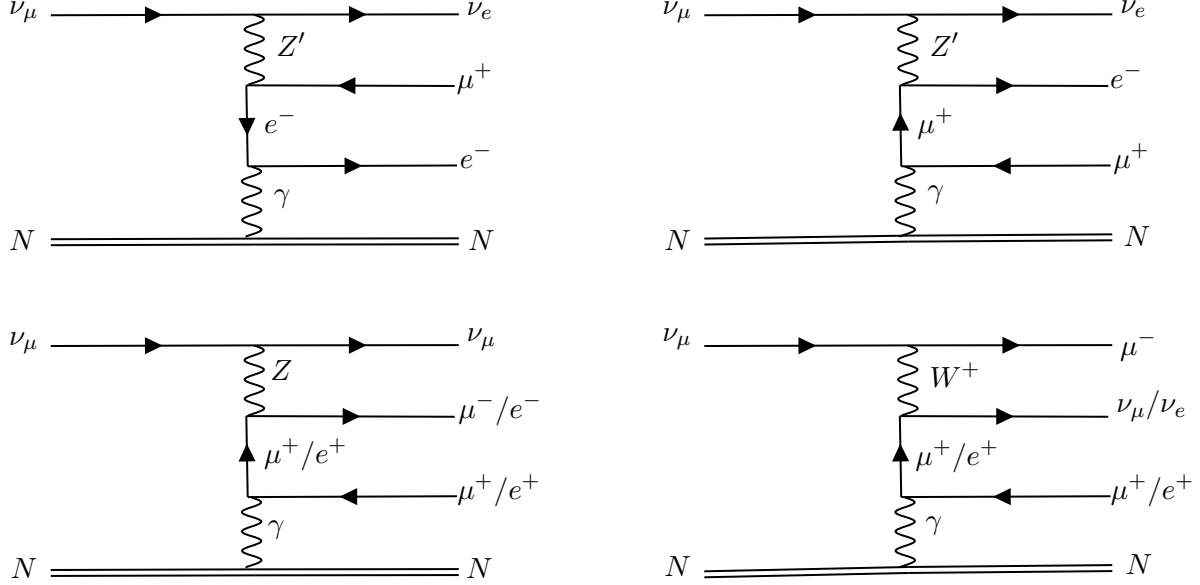


FIG. 8: Top panels: Feynman diagrams illustrating the neutrino trident process ( $\nu_\mu + N$ ) featuring off-diagonal lepton flavor violation (LFV) interactions. Lower panels: The muon neutrino trident process mediated by the SM electroweak interactions through  $W/Z$  exchange. In the latter, photon couplings with negatively charged leptons diagrams are omitted.

$e^-(p_2)$ ) based on EPA method [96, 97] will be expressed as follows<sup>2</sup> [98–100],

$$\begin{aligned} \mathcal{M}_1 &= g_{e\mu} e \bar{u}(p2) \left( \epsilon^\mu \gamma_\mu \cdot \frac{g^{\alpha\beta} - \frac{k^\alpha k^\beta}{M_{Z'}^2}}{k^2 - M_{Z'}^2} \frac{\gamma \cdot (p_1 - q) + m_\mu \gamma^\alpha}{(p_1 - q)^2 - m_\mu^2} \right. \\ &\quad \left. + \epsilon^\mu \gamma_\mu \cdot \frac{g^{\alpha\beta} - \frac{k^\alpha k^\beta}{M_{Z'}^2}}{k^2 - M_{Z'}^2} \frac{\gamma \cdot (p_2 - q) + m_e \gamma^\alpha}{(p_2 - q)^2 - m_e^2} \right) v(p_1), \end{aligned} \quad (32)$$

$$\mathcal{M}_2 = g_{e\mu} \bar{u}(k_2) \gamma^\beta u(k_1), \quad (33)$$

$$d\sigma_{\nu_\mu \gamma}^{Z'} \approx \frac{1}{2s} \frac{1}{2s} \frac{dt}{2\pi} \frac{dl}{4\pi} v |\mathcal{M}_{\nu_\mu \gamma \rightarrow \nu_e \mu^+ e^-}|^2, \quad (34)$$

In the above expression  $k = k_1 - k_2$ , and the velocity  $v$  is defined as  $v = \frac{l - m_\mu^2}{l + m_\mu^2}$  where  $m_e \rightarrow 0$ . Here,  $l$  represents the invariant momentum squared of the  $\mu$  and  $e$ , given by  $l = (P_{\mu^+} + P_{e^-})^2$ . The resulting amplitude is formulated to exclude terms involving  $m_\mu$ , as they are deemed negligible compared to other contributions. Subsequently, we reformulate the momentum

<sup>2</sup> The EPA method is valid for dimuon channels when the neutrino energy exceeds 20 GeV [49]. For mixed flavor states, it shows a factor of two enhancement against the full 2-to-4 calculations. To account for this, we adjust the cross-section enhancement applying a factor of one-half for large neutrino energy ( $E_\nu > 20$  GeV).

products using new Mandelstam variables [99] (refer to the Appendix B for details). After integrating out  $t$  and  $l$ , we obtain the following expression when  $m_\mu < M_{Z'} < \sqrt{s}$ ,

$$\sigma_{\nu_\mu\gamma}^{Z'} \simeq \frac{1}{M_{Z'}^2} \frac{g_{e\mu}^4 \alpha_{\text{EM}}}{2\pi^2} \log \left( \frac{M_{Z'}^2}{m_\mu^2} \right), \quad (35)$$

while for  $M_{Z'} < m_\mu < \sqrt{s}$ , the cross-section can be simplified as follows,

$$\sigma_{\nu_\mu\gamma}^{Z'} \simeq \frac{1}{m_\mu^2} \frac{2 g_{e\mu}^4 \alpha_{\text{EM}}}{5\pi^2} \log \left( \frac{m_\mu^2}{M_{Z'}^2} \right), \quad (36)$$

Thus, the total cross-section for the neutrino trident production with distinctive  $Z'$  signals can be expressed as follows,

$$\begin{aligned} \sigma(\nu_\mu + N \rightarrow \nu_e + \mu^+ + e^- + N) &\approx \frac{Z^2 \alpha_{\text{EM}}}{\pi} \int_{s_{\text{Min}}}^{s_{\text{Max}}} \frac{1}{s} ds \int_{q_{\text{Min}}^2}^{q_{\text{Max}}^2} dq^2 \frac{1}{q^2} F^2(A, q^2) \sigma_{\nu_\mu\gamma}^{Z'}, \quad (37) \\ q_{\text{Max}}^2 &\sim \left( \frac{m_\pi}{A^{1/3}} \right)^2, \quad q_{\text{Min}}^2 = \left( \frac{s}{2E_\nu} \right)^2, \\ s_{\text{Max}} &= 2E_\nu q_{\text{Max}}, \quad s_{\text{Min}} = m_\mu^2, \end{aligned} \quad (38)$$

where  $Z, A$  are the relevant atomic number and atomic mass of the material in the target and we adopted the electromagnetic nucleus form factor  $F(A, q^2) = \exp\left\{-\frac{(1.3\text{fm } A^{1/3})^2 q^2}{10}\right\}$  as in Ref. [100]. We used the full  $\sigma_{\nu_\gamma}^{Z'}$  results to evaluate the expected  $Z'$  signals. Since the process is essentially background free, the number expected events would be proposed statistically three events at 95% C.L. The number of coherent events will be obtained by the following form [90],

$$N_{\text{trident}} = F_{\nu_\mu} \sigma(\nu_\mu N \rightarrow \nu_e \mu^+ e^- N) \frac{M_{\text{detector}}}{M_{\text{target atom}}} N_{\text{POT}}. \quad (39)$$

where  $F_{\nu_\mu}$  is the integrated  $\nu_\mu$  flux correspond to the incoming  $\nu_\mu$  energy beam, and  $N_{\text{POT}}$  is the number of protons on target. The expected events are assumed to have 100% efficiency, with searches covering 86% of the mixing flavor states [49], resulting in negligible differences in the outcomes. For the DUNE experiment, the values are given by  $F_{\nu_\mu} = 1.04 \times 10^{-3} \text{ m}^{-2} \text{ POT}^{-1}$  and  $N_{\text{POT}} = 1.1 \times 10^{21} \text{ POT}$  per year. The ratio  $M_{\text{detector}}/M_{\text{target atom}}$  is correlated with DUNE's argon liquid detector (LArTPC) mass (147 tonnes) and atomic mass number ( $A = 40$ ). In this study, our focus lies on the DUNE experiment in general, with the anticipation that estimations for other experiments would be similar.

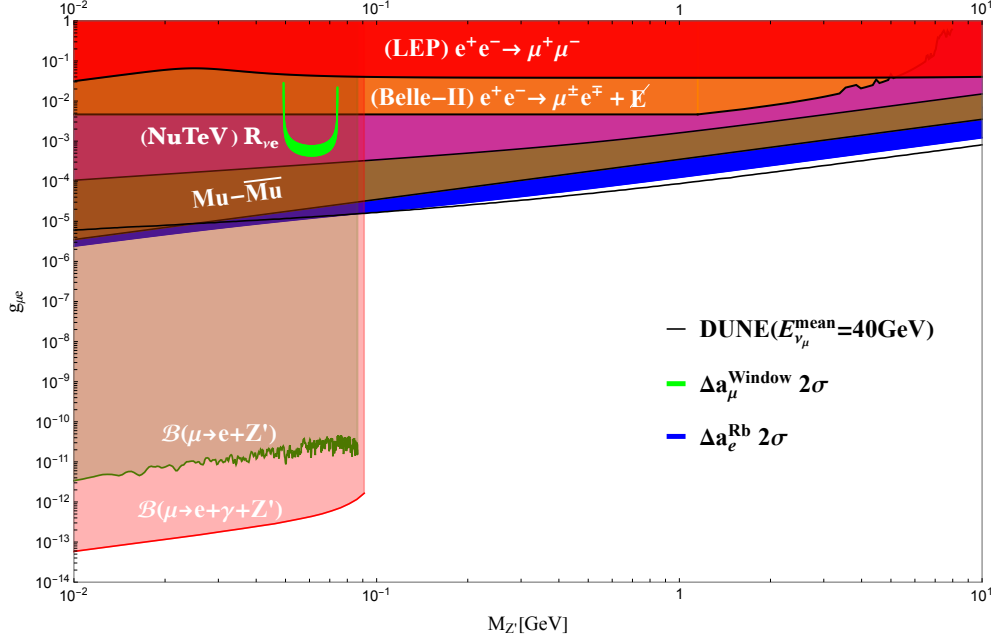


FIG. 9: The exclusion limit in the  $(M_{Z'}, g_{e\mu})$  parameter space under various constraints. The blue region denotes  $\Delta a_e(2\sigma)$ . The green band indicates the  $\Delta a_\mu(2\sigma)$ . The exclusion of  $\text{Mu} - \overline{\text{Mu}}$  oscillation is represented by the brown region [84], while the black line depicts the exclusion limits for DUNE with mean  $\nu_\mu$  energy of 40 GeV [90]. The top red region is exclusion from the LEP ( $e^+e^- \rightarrow \mu^+\mu^-$ ) at  $\sqrt{s} = 189$  GeV [65] and the orange region is Belle-II exclusion from ( $e^+e^- \rightarrow \mu^\pm e^\mp + \cancel{E}$ ) [64]. The inverse  $\mu$  decay mode from the NuTeV search, providing the ratio  $R_{\nu e}$  (eq. (27)), is labeled in magenta region [82]. The dark green line labels the exclusion region from  $\mathcal{B}(\mu \rightarrow e + X)$  [73]. The most stringent constraints for  $g_{e\mu}$  below  $m_\mu$  originate from  $\mathcal{B}(\mu \rightarrow e + \gamma + X)$  (red) [76].

#### IV. RESULTS

To verify the bounds for  $g_{e\mu}$  and  $M_{Z'}$ , we adopted the Lagrangian generated by the FeynRules [101] and using the Madgraph5 [102] to calculate the LFV three-body decay and cross section results to compare with the measurements. The decay widths of  $Z'$  and analytical evaluations are obtained by using the FeynArt [103] and FeynCalc [104–106]. Since our focus is within the mass range of 0.01 GeV to 10 GeV, we do not consider the constraints from BBN and cosmology.

The constraints of  $g_{e\mu}$  versus  $M_{Z'}$  are shown in Fig. 9. For the collider approach, the LEP measurement of  $\sigma(e^+e^- \rightarrow \mu^+\mu^-)$  [65] has labeled the top red region, while the orange

region is excluded by Belle-II ( $e^+e^- \rightarrow \mu^\pm e^\mp + \cancel{E}$ ) [64]. For the  $e^+e^- \rightarrow \mu^+\mu^-$  process, the exclusion bound remains flat for  $M_{Z'} > m_\mu$ , primarily due to the dominant effect of the  $1/s$  term. However, as  $M_{Z'}$  decreases further, the enhancement of  $1/M_{Z'}^2$  dominates, results in a reduction of the cross-section, leading to tighter limits as  $M_{Z'}$  approaches  $m_e$ . This tightening effect is attributed to the  $1/(t - M_{Z'}^2)$  from new physics diagram.

The magenta and brown areas represent exclusion regions for inverse  $\mu$  decay ratio  $R_{\nu e}$ , defined by equation eq. (27) and Mu- $\overline{\text{Mu}}$  oscillation [84], respectively. From the simplified analytical formulas eqs. (28 and 29), the constraints are proportional to  $g_{e\mu}^4/M_{Z'}^2$ , with an additional  $1/s$  suppression for  $M_{Z'} < \sqrt{s}$  and to  $g_{e\mu}^4/M_{Z'}^4$  for  $M_{Z'} > \sqrt{s}$ . Meanwhile, the limit from the brown region is proportional to  $g_{e\mu}^2/M_{Z'}^2$ , leading to a linear enhancement of the bounds as  $M_{Z'} \rightarrow m_e$ .

The green band shows the  $2\sigma$  allowed range of  $\Delta a_\mu$ . We see that the  $Z'$  itself with  $e - \mu$  couplings can only resolve the discrepancy  $\Delta a_\mu$  within small mass region ( $0.04 \text{ GeV} < M_{Z'} < 0.08 \text{ GeV}$ ) while the experimental constraints have already ruled out this scenario.

In the context of the neutrino trident process, the DUNE experiment estimates the significance with a solid black line for a mean neutrino energy of  $E_{\nu_\mu} = 40 \text{ GeV}$ . The exclusion region from trident events is slightly more stringent than that from  $\Delta a_e$ , as indicated by the plot. From eqs. (35 and 36), the cross-sections exhibit dependencies proportional to  $g_{e\mu}^4 \log(1/M_{Z'}^2)$  and  $g_{e\mu}^4/M_{Z'}^2 \log(M_{Z'}^2)$ , respectively. As  $M_{Z'}$  increases from below  $m_\mu$  to around 10 GeV, the constraint curve transitions smoothly, reflecting the enhanced cross-section when  $M_{Z'} < m_\mu$  due to the logarithmic term  $\log(1/M_{Z'}^2)$ , which strengthens the coupling limit  $g_{e\mu}$ . Conversely, the trident cross-section is suppressed as  $M_{Z'}$  exceeds  $m_\mu$  owing to the inverse-square dependence  $1/M_{Z'}^2$ , resulting in a weaker constraint on the coupling.

Based on the plot, it is apparent that the most stringent constraint arises from the  $\mathcal{B}(\mu \rightarrow e + \gamma + Z')$  process when  $M_{Z'} < m_\mu$ . This limitation stems from the  $M_{Z'}$  enhancement in the denominator, an extra factor of  $\alpha_{\text{EM}}$ , and the suppression of the three-body phase space, which includes an additional factor related to the density of states when integrating the final momenta of the particles,  $\prod_{i=1}^3 \frac{d^3 \vec{p}_i}{(2\pi)^3}$ . Therefore, considering these exclusion limits, we anticipate that the neutrino trident experiment will capitalize on its background-free signal, thereby offering a promising avenue to explore maximal LFV  $Z'$ .

## V. CONCLUSIONS

In this work, we investigated a novel  $U(1)'$  gauge symmetry, focusing on the  $Z'$  boson that couples with  $e$  and  $\mu$  through a specific charge configuration. We propose a UV model featuring four scalars—three doublets and one singlet—that contribute to the  $M_{Z'}$  after symmetry breaking, without altering the SM  $Z$  boson mass. The model employs a discrete symmetry  $\ell_{1L} \rightarrow \ell_{2L}$ ,  $e_{1R} \rightarrow e_{2R}$ ,  $Z'_\mu \rightarrow -Z'_\mu$ , leading to maximally off-diagonal interactions between  $Z'$  and leptons, manifesting exclusively as lepton flavor-violating (LFV) processes. A notable aspect indicates that the Yukawa coupling between  $\mu/e$  and the SM Higgs remains identical. Given recent measurements of the Higgs' leptonic decay branching ratios, we anticipate that future precision measurements will be sensitive to this model.

Next, we analyzed the existing experiments aimed at constraining the LFV coupling  $g_{e\mu}$  of  $Z'$ . Specifically, the discrepancy between the SM prediction and the measured magnetic moment of the muon,  $\Delta a_\mu$ , cannot be explained by the  $Z'$ , as the parameter space where  $Z'$  could account for this discrepancy has already been ruled out by other experimental measurements. We considered several LFV search limits, including those from Belle-II, LEP, LFV decays, inverse muon decay, Muonium-anti Muonium oscillation, and the newly proposed neutrino trident process ( $\nu_\mu + N \rightarrow \nu_e + \mu^+ + e^- + N$ ).

Neutrino trident processes are measured from the DUNE and some other similar experiments to test the LFV interaction. Most searches have focused on muon pair final states. However, the LFV interaction involve the maximal flavor violation can contribute a distinctive signal  $\mu^+e^-$  from  $\nu_\mu$  beams without any SM background as the SM does not produce  $\mu^+e^-$  in the final state via  $\nu_\mu$ . We employed the neutrino trident production method to investigate the  $Z'\mu^+e^-$  vertex, utilizing its framework to incorporate the amplitude of a distinct, background-free signal through the DUNE experiment. In the appendix, we listed the kinematic variables for the 2-to-3 scattering process  $\nu_\mu + \gamma \rightarrow \nu_e + \mu^+ + e^-$  and calculated the final cross-section for an initial  $\nu_\mu$  collides with the nucleus. The resulting constraint on  $Z'$  is stricter compared to those from colliders and LFV decays when  $M_{Z'} > m_\mu$ , with the limit forming a quadratic curve. For  $M_{Z'} < m_\mu$ , the primary constraint comes from  $\mathcal{B}(\mu \rightarrow e + \gamma + Z')$  due to the enhancement by the factor  $m_\mu^3/M_{Z'}^2$ , and the suppression both from the three-body phase space factor and QED coupling  $\alpha_{\text{EM}}$ .

## Appendix A: Scalar potential with neutral scalars

The scalar potential can be expressed as follows, incorporating the discrete symmetry ( $\phi_1 \rightarrow \phi_2$ ) [23],

$$\begin{aligned}
V_{\phi_1, \phi_2, \phi_3, \phi_4} = & \lambda_1(\phi_3^\dagger \phi_3 - v_3^2)^2 + \lambda_2(\phi_1^\dagger \phi_1 + \phi_2^\dagger \phi_2 - 2v_0^2)^2 \\
& + \lambda_3(\phi_1^\dagger \phi_1 - \phi_2^\dagger \phi_2)^2 + \lambda_4(\phi_1^\dagger \phi_1 + \phi_2^\dagger \phi_2 + \phi_3^\dagger \phi_3 - v_3^2 - 2v_0^2)^2 \\
& + \lambda_5[\phi_1^\dagger \phi_1 \phi_2^\dagger \phi_2 - \phi_1^\dagger \phi_2 \phi_2^\dagger \phi_1] \\
& + \lambda_6[\phi_3^\dagger \phi_3 (\phi_1^\dagger \phi_1 + \phi_2^\dagger \phi_2) - \phi_3^\dagger \phi_1 \phi_1^\dagger \phi_3 - \phi_3^\dagger \phi_2 \phi_2^\dagger \phi_3] \\
& + \lambda_7[\phi_3^\dagger \phi_3 (\phi_1^\dagger \phi_1 + \phi_2^\dagger \phi_2) - \phi_3^\dagger \phi_1 \phi_3^\dagger \phi_2 - \phi_1^\dagger \phi_3 \phi_2^\dagger \phi_3] \\
& + \frac{1}{2}\mu_4^2 \phi_4^2 + \lambda_{44} \phi_4^4,
\end{aligned} \tag{A1}$$

Based on the aforementioned reference and the alteration of our set up, one can redefine the CP-even scalar components,

$$S_1 = \frac{\rho_1 + \rho_2}{\sqrt{2}}, S_2 = \frac{\rho_1 - \rho_2}{\sqrt{2}}, \tag{A2}$$

The CP even squared mass matrices can be expressed as follows ( $v_0 \equiv v_1 = v_2$ ),

$$M_{S_1}^2 = 8v_0^2 \lambda_2, \tag{A3}$$

$$M_{S_2}^2 = 8\lambda_3 v_0^2 + 2v_3^2 \lambda_7, \tag{A4}$$

$$M_H^2 = 4v_3^2 \lambda_1, \tag{A5}$$

$$M_{S_4}^2 = \frac{1}{2}(\mu_4^2 + 8v_4^2 \lambda_{44}), \tag{A6}$$

The above  $M_H$  would be the SM Higgs mass, with the flavor states and mass states being identical ( $\rho_1, \rho_2, \rho_3, \rho_4 \rightarrow S_1, S_2, H, S_4$ ) when we assume  $\lambda_4 \rightarrow 0$ . If  $\lambda_4 \neq 0$ , one could have non-diagonalized mass matrices,

$$M_{S_1, \rho_3}^2 = \begin{pmatrix} 8v_0^2(\lambda_2 + \lambda_4) & 4\sqrt{2}v_0v_3\lambda_4 \\ 4\sqrt{2}v_0v_3\lambda_4 & 4v_3^2(\lambda_1 + \lambda_4) \end{pmatrix}, \tag{A7}$$

On the other hand,  $M_{S_2}^2$  and  $M_{S_4}^2$  are automatically diagonalized as shown in eqs. (A4) and (A6), with  $S_2, S_4$  representing the mass states. The states ( $S_1$  and  $\rho_3$ ) are no longer directly equivalent to their mass eigenstates. Instead, the mass eigenstates ( $S'_1$  and  $H$ ) are introduced, and their relationship can be expressed through the following 2-by-2 mixing

matrix, which rotates from the flavor states  $S_1$  and  $\rho_3$  to the mass states  $S'_1$  and  $H$ ),

$$\begin{pmatrix} S_1 \\ \rho_3 \end{pmatrix} = \begin{pmatrix} \frac{\sqrt{2}v_0v_3\lambda_4}{v_3^2\lambda_1-2v_0^2\lambda_2} & 1 \\ 1 & \frac{-\sqrt{2}v_0v_3\lambda_4}{-v_3^2\lambda_1+2v_0^2\lambda_2} \end{pmatrix} \begin{pmatrix} H \\ S'_1 \end{pmatrix} + \mathcal{O}(\lambda_4^2), \quad (\text{A8})$$

Thus, the flavor states  $(\rho_1, \rho_2, \rho_3, \rho_4)$  transform into the physical mass states  $(S'_1, S_2, H, S_4)$  resembles the SM-like Higgs ( $H$ ).

In this context, we exclusively focus on the CP-even scalars due to their correlation with SM-like scalar Yukawa couplings. The CP-odd and charged components are not pertinent to our current discussion. The scalar potential introduces numerous parameters, resulting in a vast parameter space that could potentially include additional scalar states, which we do not investigate here.

## Appendix B: Kinematic variables for the neutrino trident process.

The kinematic variables that transform the 4-momentum product into Mandelstam variables in the 2-to-3 neutrino trident production ( $\nu_\mu(k_1) + \gamma(q) \rightarrow \nu_e(k_2) + \mu^+(p_1) + e^-(p_2)$ )

are expressed as follows:

$$k_1 + q = k_2 + p_1 + p_2, \quad (B1)$$

$$k_1^2 = k_2^2 = 0, \quad k = k_1 - k_2, \quad (B2)$$

$$\kappa_1 = m_\mu^2 - p_1^2, \quad \kappa_2 = -p_2^2, \quad (B3)$$

$$s = (k_1 + q)^2, \quad l = (p_1 + p_2)^2, \quad t = 2k \cdot q = \kappa_1 + \kappa_2 = l - k^2 - q^2, \quad (B4)$$

$$\kappa_1 \rightarrow \frac{t}{2} \left( 1 + \frac{m_\mu^2}{l} + x \left( 1 - \frac{m_\mu^2}{l} \right) \right), \quad (B5)$$

$$\kappa_2 \rightarrow \frac{t}{2} \left( 1 - \frac{m_\mu^2}{l} - x \left( 1 - \frac{m_\mu^2}{l} \right) \right), \quad (B6)$$

$$\kappa_3 \rightarrow l - t, \quad (B7)$$

$$k_1 \cdot q \rightarrow \frac{s}{2}, \quad k_2 \cdot q \rightarrow \frac{s-t}{2}, \quad p_1 \cdot q \rightarrow \frac{\kappa_1}{2}, \quad p_2 \cdot q \rightarrow \frac{\kappa_2}{2}, \quad (B8)$$

$$k_1 \cdot p_1 \rightarrow \frac{l - \kappa_1}{2} + \frac{s-l}{4} \left( 1 + \frac{m_\mu^2}{l} + x \left( 1 - \frac{m_\mu^2}{l} \right) \right), \quad (B9)$$

$$k_1 \cdot p_2 \rightarrow \frac{l - \kappa_2}{2} + \frac{s-l}{4} \left( 1 - \frac{m_\mu^2}{l} - x \left( 1 - \frac{m_\mu^2}{l} \right) \right), \quad (B10)$$

$$k_2 \cdot p_1 \rightarrow \frac{s-l}{4} \left( 1 + \frac{m_\mu^2}{l} + x \left( 1 - \frac{m_\mu^2}{l} \right) \right), \quad (B11)$$

$$k_2 \cdot p_2 \rightarrow \frac{s-l}{4} \left( 1 - \frac{m_\mu^2}{l} - x \left( 1 - \frac{m_\mu^2}{l} \right) \right), \quad (B12)$$

$$p_1 \cdot p_2 \rightarrow \frac{l}{2} - m_\mu^2, \quad k_1 \cdot k_2 \rightarrow -\frac{\kappa_3}{2}. \quad (B13)$$

We employed the notations introduced in Ref. [99], where  $x = v \cos \theta_{qp_1}$ , with  $v$  representing the velocity of the muon in the center-of-mass (COM) frame of the  $\mu^+(p_1)e^-(p_2)$  pair, and we take  $q^2 \rightarrow 0$ . In these expressions, the electron mass is neglected as it remains the lightest particle regardless of the value of  $M_{Z'}$ .

### Acknowledgments

We thank Jinhui Guo and Yuxuan He for their discussion on the early stage of the work. The work of JL is supported by Natural Science Foundation of China under grant No.

- [1] G. Feinberg, P. Kabir and S. Weinberg, *Transformation of muons into electrons*, *Phys. Rev. Lett.* **3** (1959) 527.
- [2] G. Feinberg and S. Weinberg, *Law of Conservation of Muons*, *Phys. Rev. Lett.* **6** (1961) 381.
- [3] V. Cirigliano, B. Grinstein, G. Isidori and M.B. Wise, *Minimal flavor violation in the lepton sector*, *Nucl. Phys. B* **728** (2005) 121 [[hep-ph/0507001](#)].
- [4] L. Calibbi and G. Signorelli, *Charged Lepton Flavour Violation: An Experimental and Theoretical Introduction*, *Riv. Nuovo Cim.* **41** (2018) 71 [[1709.00294](#)].
- [5] F. Björkeroth, E.J. Chun and S.F. King, *Flavourful Axion Phenomenology*, *JHEP* **08** (2018) 117 [[1806.00660](#)].
- [6] C. Cornellà, P. Paradisi and O. Sumensari, *Hunting for ALPs with Lepton Flavor Violation*, *JHEP* **01** (2020) 158 [[1911.06279](#)].
- [7] L. Calibbi, D. Redigolo, R. Ziegler and J. Zupan, *Looking forward to lepton-flavor-violating ALPs*, *JHEP* **09** (2021) 173 [[2006.04795](#)].
- [8] K. Cheung, A. Soffer, Z.S. Wang and Y.-H. Wu, *Probing charged lepton flavor violation with axion-like particles at Belle II*, *JHEP* **11** (2021) 218 [[2108.11094](#)].
- [9] L. Calibbi, T. Li, L. Mukherjee and Y. Yang, *Probing ALP Lepton Flavour Violation at  $\mu$ TRISTAN*, [2406.13234](#).
- [10] H. Davoudiasl, R. Marcarelli and E.T. Neil, *Flavor-violating ALPs, electron g-2, and the Electron-Ion Collider*, *Phys. Rev. D* **109** (2024) 115013 [[2402.17821](#)].
- [11] J. Hisano, T. Moroi, K. Tobe and M. Yamaguchi, *Lepton flavor violation via right-handed neutrino Yukawa couplings in supersymmetric standard model*, *Phys. Rev. D* **53** (1996) 2442 [[hep-ph/9510309](#)].
- [12] A. Abada, M.E. Krauss, W. Porod, F. Staub, A. Vicente and C. Weiland, *Lepton flavor violation in low-scale seesaw models: SUSY and non-SUSY contributions*, *JHEP* **11** (2014) 048 [[1408.0138](#)].
- [13] M. Blanke, A.J. Buras, B. Duling, A. Poschenrieder and C. Tarantino, *Charged Lepton Flavour Violation and (g-2)(mu) in the Littlest Higgs Model with T-Parity: A Clear Distinction from Supersymmetry*, *JHEP* **05** (2007) 013 [[hep-ph/0702136](#)].

[14] X. Han, *The Lepton Flavor Violating Decays  $Z \rightarrow l_i l_j$  in the Simplest little Higgs Model*, *Mod. Phys. Lett. A* **27** (2012) 1250158 [[1104.3534](#)].

[15] M. Ardu, S. Davidson and S. Lavignac, *Distinguishing models with  $\mu \rightarrow e$  observables*, *JHEP* **11** (2023) 101 [[2308.16897](#)].

[16] W. Altmannshofer, P. Munbodh and T. Oh, *Probing lepton flavor violation at Circular Electron-Positron Colliders*, *JHEP* **08** (2023) 026 [[2305.03869](#)].

[17] W. Altmannshofer, C. Caillol, M. Dam, S. Xella and Y. Zhang, *Charged Lepton Flavour Violation in Heavy Particle Decays*, in *Snowmass 2021*, 5, 2022 [[2205.10576](#)].

[18] J.-P. Huo, X.-X. Dong, J. Ma, S.-M. Zhao, C. Guo, H.-B. Zhang et al., *Lepton flavor violating decays  $Z \rightarrow l_i^\pm l_j^\mp$  in the B-L Supersymmetric Standard Model*, [2406.03108](#).

[19] T. Toma and A. Vicente, *Lepton Flavor Violation in the Scotogenic Model*, *JHEP* **01** (2014) 160 [[1312.2840](#)].

[20] Tapender, S. Verma and S. Kumar, *On Lepton Flavor Violation and Dark Matter in Scotogenic model with Trimaximal Mixing*, [2402.16491](#).

[21] X.-G. He, G.C. Joshi, H. Lew and R.R. Volkas, *Simplest  $Z'$  model*, *Phys. Rev. D* **44** (1991) 2118.

[22] X.G. He, G.C. Joshi, H. Lew and R.R. Volkas, *New- $Z'$  phenomenology*, *Phys. Rev. D* **43** (1991) R22.

[23] R. Foot, X.G. He, H. Lew and R.R. Volkas, *Model for a light  $Z$ -prime boson*, *Phys. Rev. D* **50** (1994) 4571 [[hep-ph/9401250](#)].

[24] S. Iguro, Y. Omura and M. Takeuchi, *Probing  $\mu\tau$  flavor-violating solutions for the muon  $g-2$  anomaly at Belle II*, *JHEP* **09** (2020) 144 [[2002.12728](#)].

[25] M. Atzori Corona, M. Cadeddu, N. Cargioli, F. Dordei, C. Giunti, Y.F. Li et al., *Probing light mediators and  $(g-2)_\mu$  through detection of coherent elastic neutrino nucleus scattering at COHERENT*, *JHEP* **05** (2022) 109 [[2202.11002](#)].

[26] A. Crivellin and S. Iguro, *Accumulating Hints for Flavour Violating Higgses at the Electroweak Scale*, [2311.03430](#).

[27] D. Espinosa-Gomez, F. Ramirez-Zavaleta and E.S. Tututi, *Decay of the  $Z'$  gauge boson with lepton flavor violation*, *Eur. Phys. J. C* **83** (2023) 909 [[2310.04509](#)].

[28] J.F. Eguren, S. Klingel, E. Stamou, M. Tabet and R. Ziegler, *Flavor Phenomenology of Light Dark Vectors*, [2405.00108](#).

[29] M. Marin, R. Gaitan and R. Martinez, *Lepton flavor-violating higgs decays mediated by ultralight gauge boson*, [2406.17040](#).

[30] Y. Cheng, X.-G. He and J. Sun, *Widening the  $U(1)_{L_\mu-L_\tau} Z'$  mass range for resolving the muon  $g-2$  anomaly*, *Phys. Lett. B* **827** (2022) 136989 [[2112.09920](#)].

[31] Z. Kang and Y. Shigekami,  *$(g-2)_\mu$  versus flavor changing neutral current induced by the light  $(B-L)_{\mu\tau}$  boson*, *JHEP* **11** (2019) 049 [[1905.11018](#)].

[32] S. Eijima, M. Ibe and K. Murai, *Muon  $g-2$  and non-thermal leptogenesis in  $U(1)_{L_\mu-L_\tau}$  model*, *JHEP* **05** (2023) 010 [[2303.09751](#)].

[33] A.J. Buras, A. Crivellin, F. Kirk, C.A. Manzari and M. Montull, *Global analysis of leptophilic  $Z'$  bosons*, *JHEP* **06** (2021) 068 [[2104.07680](#)].

[34] ATLAS collaboration, *A search for lepton-flavor-violating decays of the  $Z$  boson into a  $\tau$ -lepton and a light lepton with the ATLAS detector*, *Phys. Rev. D* **98** (2018) 092010 [[1804.09568](#)].

[35] T. Araki, K. Asai, H. Otono, T. Shimomura and Y. Takubo, *Search for lepton flavor violating decay at FASER*, *JHEP* **01** (2023) 145 [[2210.12730](#)].

[36] CDF collaboration, *Search for Maximal Flavor Violating Scalars in Same-Charge Lepton Pairs in  $p\bar{p}$  Collisions at  $\sqrt{s} = 1.96$ -TeV*, *Phys. Rev. Lett.* **102** (2009) 041801 [[0809.4903](#)].

[37] P. Foldenauer and J. Jaeckel, *Purely flavor-changing  $Z'$  bosons and where they might hide*, *JHEP* **05** (2017) 010 [[1612.07789](#)].

[38] J. Kriewald, J. Orloff, E. Pinsard and A.M. Teixeira, *Prospects for a flavour violating  $Z'$  explanation of  $\Delta a_{\mu,e}$* , *Eur. Phys. J. C* **82** (2022) 844 [[2204.13134](#)].

[39] R. Ding, J. Li, M. Lu, Z. You, Z. Wang and Q. Li, *Study of charged Lepton Flavor Violation in electron muon interactions*, [2405.09417](#).

[40] S. Bar-Shalom and A. Rajaraman, *Models and phenomenology of maximal flavor violation*, *Phys. Rev. D* **77** (2008) 095011 [[0711.3193](#)].

[41] CHARM-II collaboration, *First observation of neutrino trident production*, *Phys. Lett. B* **245** (1990) 271.

[42] CCFR collaboration, *Neutrino Tridents and  $W Z$  Interference*, *Phys. Rev. Lett.* **66** (1991) 3117.

[43] NuTeV collaboration, *Evidence for diffractive charm production in muon-neutrino Fe and anti-muon-neutrino Fe scattering at the Tevatron*, *Phys. Rev. D* **61** (2000) 092001

[hep-ex/9909041].

- [44] W. Czyz, G.C. Sheppey and J.D. Walecka, *Neutrino production of lepton pairs through the point four-fermion interaction*, *Nuovo Cim.* **34** (1964) 404.
- [45] K. Fujikawa, *The self-coupling of weak lepton currents in high-energy neutrino and muon reactions*, *Annals Phys.* **68** (1971) 102.
- [46] R. Francener, V.P. Goncalves and D.R. Gratieri, *Neutrino trident scattering at the LHC energy regime*, [2406.13593](#).
- [47] W. Altmannshofer, T. Mäkelä, S. Sarkar, S. Trojanowski, K. Xie and B. Zhou, *Discovering neutrino tridents at the Large Hadron Collider*, [2406.16803](#).
- [48] S.-F. Ge, M. Lindner and W. Rodejohann, *Atmospheric Trident Production for Probing New Physics*, *Phys. Lett. B* **772** (2017) 164 [[1702.02617](#)].
- [49] P. Ballett, M. Hostert, S. Pascoli, Y.F. Perez-Gonzalez, Z. Tabrizi and R. Zukanovich Funchal, *Neutrino Trident Scattering at Near Detectors*, *JHEP* **01** (2019) 119 [[1807.10973](#)].
- [50] ATLAS collaboration, *A detailed map of Higgs boson interactions by the ATLAS experiment ten years after the discovery*, *Nature* **607** (2022) 52 [[2207.00092](#)].
- [51] CMS collaboration, *A portrait of the Higgs boson by the CMS experiment ten years after the discovery*, *Nature* **607** (2022) 60 [[2207.00043](#)].
- [52] CMS collaboration, *Search for the Higgs boson decay to a pair of electrons in proton-proton collisions at  $\sqrt{s} = 13\text{TeV}$* , *Phys. Lett. B* **846** (2023) 137783 [[2208.00265](#)].
- [53] M. Cè et al., *Window observable for the hadronic vacuum polarization contribution to the  $(g-2)_\mu$  from lattice QCD*, *Phys. Rev. D* **106** (2022) 114502 [[2206.06582](#)].
- [54] G. Colangelo, A.X. El-Khadra, M. Hoferichter, A. Keshavarzi, C. Lehner, P. Stoffer et al., *Data-driven evaluations of Euclidean windows to scrutinize hadronic vacuum polarization*, *Phys. Lett. B* **833** (2022) 137313 [[2205.12963](#)].
- [55] H. Acaroğlu, M. Blanke and M. Tabet, *Opening the Higgs portal to lepton-flavoured dark matter*, *JHEP* **11** (2023) 079 [[2309.10700](#)].
- [56] MUON G-2 collaboration, *Measurement of the Positive Muon Anomalous Magnetic Moment to 0.20 ppm*, *Phys. Rev. Lett.* **131** (2023) 161802 [[2308.06230](#)].
- [57] G. Armando, P. Panci, J. Weiss and R. Ziegler, *Leptonic ALP portal to the dark sector*, *Phys. Rev. D* **109** (2024) 055029 [[2310.05827](#)].
- [58] S. Borsanyi et al., *Leading hadronic contribution to the muon magnetic moment from lattice*

*QCD*, *Nature* **593** (2021) 51 [[2002.12347](#)].

[59] G.F. Giudice, P. Paradisi and M. Passera, *Testing new physics with the electron g-2*, *JHEP* **11** (2012) 113 [[1208.6583](#)].

[60] L. Morel, Z. Yao, P. Cladé and S. Guellati-Khélifa, *Determination of the fine-structure constant with an accuracy of 81 parts per trillion*, *Nature* **588** (2020) 61.

[61] X. Fan, T.G. Myers, B.A.D. Sukra and G. Gabrielse, *Measurement of the Electron Magnetic Moment*, *Phys. Rev. Lett.* **130** (2023) 071801 [[2209.13084](#)].

[62] R.H. Parker, C. Yu, W. Zhong, B. Estey and H. Müller, *Measurement of the fine-structure constant as a test of the Standard Model*, *Science* **360** (2018) 191 [[1812.04130](#)].

[63] H.H. Patel, *Package-X: A Mathematica package for the analytic calculation of one-loop integrals*, *Comput. Phys. Commun.* **197** (2015) 276 [[1503.01469](#)].

[64] BELLE-II collaboration, *Search for an Invisibly Decaying Z' Boson at Belle II in  $e^+e^- \rightarrow \mu^+\mu^- (e^\pm\mu^\mp) + \not{E}$  Final States*, *Phys. Rev. Lett.* **124** (2020) 141801 [[1912.11276](#)].

[65] DELPHI collaboration, *Measurement and interpretation of fermion-pair production at LEP energies of 183-GeV and 189-GeV*, *Phys. Lett. B* **485** (2000) 45 [[hep-ex/0103025](#)].

[66] F. Renga, *Experimental searches for muon decays beyond the Standard Model*, *Rev. Phys.* **4** (2019) 100029 [[1902.06291](#)].

[67] MEG collaboration, *New limit on the lepton-flavour violating decay  $\mu^+ \rightarrow e^+\gamma$* , *Phys. Rev. Lett.* **107** (2011) 171801 [[1107.5547](#)].

[68] MEG collaboration, *New constraint on the existence of the  $\mu^+ \rightarrow e^+\gamma$  decay*, *Phys. Rev. Lett.* **110** (2013) 201801 [[1303.0754](#)].

[69] MEG collaboration, *Search for the lepton flavour violating decay  $\mu^+ \rightarrow e^+\gamma$  with the full dataset of the MEG experiment*, *Eur. Phys. J. C* **76** (2016) 434 [[1605.05081](#)].

[70] SINDRUM collaboration, *Search for the Decay  $\mu^+ \rightarrow e^+e^+e^-$* , *Nucl. Phys. B* **299** (1988) 1.

[71] MU3E collaboration, *Technical design of the phase I Mu3e experiment*, *Nucl. Instrum. Meth. A* **1014** (2021) 165679 [[2009.11690](#)].

[72] MU3E collaboration, *Searching for Charged Lepton Flavour Violation with Mu3e $^\dagger$* , *Phys. Sci. Forum* **8** (2023) 30 [[2308.11403](#)].

[73] TWIST collaboration, *Search for two body muon decay signals*, *Phys. Rev. D* **91** (2015) 052020 [[1409.0638](#)].

[74] R. Bilger, K. Foehl, H. Clement, M. Croni, A. Erhardt, R. Meier et al., *Search for exotic*

muon decays, *Phys. Lett. B* **446** (1999) 363 [[hep-ph/9811333](#)].

[75] PARTICLE DATA GROUP collaboration, *Review of Particle Physics*, *PTEP* **2022** (2022) 083C01.

[76] J.T. Goldman et al., *Light Boson Emission in the Decay of the  $\mu^+$* , *Phys. Rev. D* **36** (1987) 1543.

[77] J. Heeck, *Lepton flavor violation with light vector bosons*, *Phys. Lett. B* **758** (2016) 101 [[1602.03810](#)].

[78] M.S. Chanowitz and M.K. Gaillard, *The tev physics of strongly interacting w's and z's*, *Nuclear Physics B* **261** (1985) 379.

[79] M.E. Peskin, *Lectures on the Theory of the Weak Interaction*, in *2016 European School of High-Energy Physics*, pp. 1–70, 2017, DOI [[1708.09043](#)].

[80] R.J. Hill, R. Plestid and J. Zupan, *Searching for new physics at  $\mu \rightarrow e$  facilities with  $\mu^+$  and  $\pi^+$  decays at rest*, *Phys. Rev. D* **109** (2024) 035025 [[2310.00043](#)].

[81] AMSTERDAM-CERN-HAMBURG-MOSCOW-ROME collaboration, *Experimental Study of Inverse Muon Decay*, *Phys. Lett. B* **93** (1980) 203.

[82] NuTeV collaboration, *Search for the Lepton Number Violating Process  $\bar{\nu}_\mu e^- \rightarrow \mu^- \bar{\nu}_e$* , *Phys. Rev. Lett.* **87** (2001) 071803 [[hep-ex/0104029](#)].

[83] T. Fukuyama, Y. Mimura and Y. Uesaka, *Models of the muonium to antimuonium transition*, *Phys. Rev. D* **105** (2022) 015026 [[2108.10736](#)].

[84] L. Willmann et al., *New bounds from searching for muonium to anti-muonium conversion*, *Phys. Rev. Lett.* **82** (1999) 49 [[hep-ex/9807011](#)].

[85] K. Koike, M. Konuma, K. Kurata and K. Sugano, *Neutrino production of lepton pairs. 1.*, *Prog. Theor. Phys.* **46** (1971) 1150.

[86] K. Koike, M. Konuma, K. Kurata and K. Sugano, *Neutrino production of lepton pairs. 2.*, *Prog. Theor. Phys.* **46** (1971) 1799.

[87] R.W. Brown, R.H. Hobbs, J. Smith and N. Stanko, *Intermediate boson. iii. virtual-boson effects in neutrino trident production*, *Phys. Rev. D* **6** (1972) 3273.

[88] SHiP collaboration, *Neutrino physics with the SHiP experiment at CERN*, *PoS EPS-HEP2019* (2020) 372.

[89] A. Di Crescenzo, *Neutrino physics and dark matter search with SHiP at CERN*, *Int. J. Mod. Phys. Conf. Ser.* **51** (2023) 2360002.

[90] W. Altmannshofer, S. Gori, J. Martín-Albo, A. Sousa and M. Wallbank, *Neutrino Tridents at DUNE*, *Phys. Rev. D* **100** (2019) 115029 [[1902.06765](#)].

[91] J.M. Conrad, M.H. Shaevitz and T. Bolton, *Precision measurements with high-energy neutrino beams*, *Rev. Mod. Phys.* **70** (1998) 1341 [[hep-ex/9707015](#)].

[92] W.K. Sakumoto et al., *Calibration of the CCFR Target Calorimeter*, *Nucl. Instrum. Meth. A* **294** (1990) 179.

[93] B.J. King et al., *Measuring Muon Momenta with the CCFR Neutrino Detector*, *Nucl. Instrum. Meth. A* **302** (1991) 254.

[94] CCFR/NUTEV collaboration, *Precision electroweak results from neutrino nucleon scattering at CCFR/NuTeV*, *Nucl. Phys. B Proc. Suppl.* **66** (1998) 112.

[95] G. Magill and R. Plestid, *Neutrino Trident Production at the Intensity Frontier*, *Phys. Rev. D* **95** (2017) 073004 [[1612.05642](#)].

[96] C.F. von Weizsäcker, *Radiation emitted in collisions of very fast electrons*, *Z. Phys.* **88** (1934) 612.

[97] E.J. Williams, *Nature of the high-energy particles of penetrating radiation and status of ionization and radiation formulae*, *Phys. Rev.* **45** (1934) 729.

[98] R. Belusevic and J. Smith, *W - Z Interference in Neutrino - Nucleus Scattering*, *Phys. Rev. D* **37** (1988) 2419.

[99] M.I. Vysotsky, I.V. Gaidenko and V.A. Novikov, *On lepton pair production in neutrino nucleus collisions*, *Phys. Atom. Nucl.* **65** (2002) 1634.

[100] W. Altmannshofer, S. Gori, M. Pospelov and I. Yavin, *Neutrino Trident Production: A Powerful Probe of New Physics with Neutrino Beams*, *Phys. Rev. Lett.* **113** (2014) 091801 [[1406.2332](#)].

[101] A. Alloul, N.D. Christensen, C. Degrande, C. Duhr and B. Fuks, *FeynRules 2.0 - A complete toolbox for tree-level phenomenology*, *Comput. Phys. Commun.* **185** (2014) 2250 [[1310.1921](#)].

[102] J. Alwall, M. Herquet, F. Maltoni, O. Mattelaer and T. Stelzer, *MadGraph 5 : Going Beyond*, *JHEP* **06** (2011) 128 [[1106.0522](#)].

[103] T. Hahn, *Generating Feynman diagrams and amplitudes with FeynArts 3*, *Comput. Phys. Commun.* **140** (2001) 418 [[hep-ph/0012260](#)].

[104] R. Mertig, M. Böhm and A. Denner, *Feyncalc - computer-algebraic calculation of feynman amplitudes*, *Computer Physics Communications* **64** (1991) 345.

- [105] V. Shtabovenko, R. Mertig and F. Orellana, *New Developments in FeynCalc 9.0*, *Comput. Phys. Commun.* **207** (2016) 432 [[1601.01167](https://arxiv.org/abs/1601.01167)].
- [106] V. Shtabovenko, R. Mertig and F. Orellana, *FeynCalc 9.3: New features and improvements*, *Comput. Phys. Commun.* **256** (2020) 107478 [[2001.04407](https://arxiv.org/abs/2001.04407)].